High density fiber postitioner system for massive spectroscopic surveys

Philipp Hörler, Luzius Kronig, Jean-Paul Kneib, Mohamed Bouri, Hannes Bleuler, Dieter von Moos

Monthly Notices
of the
ROYAL ASTRONOMICAL SOCIETY

MNRAS **481,** 3070–3082 (2018)
Advance Access publication 2018 September 10

doi:10.1093/mnras/sty2442

High density fiber postitioner system for massive spectroscopic surveys

Philipp Hörler,[1]★ Luzius Kronig,[1] Jean-Paul Kneib,[2,3] Mohamed Bouri,[1] Hannes Bleuler[1] and Dieter von Moos[4]

[1]*Laboratoire de systèmes robotiques, École polytechnique fèdèrale de Lausanne, CH-1015 Lausanne, Switzerland*
[2]*Laboratory of Astrophysics, Ecole Polytechnique Fèdèrale de Lausanne, Observatoire de Sauverny, CH-1290 Versoix, Switzerland*
[3]*Aix Marseille Universitè, CNRS, LAM (Laboratoire d'Astrophysique de Marseille) UMR 7326, F-13388 Marseille, France*
[4]*Maxon Motor AG, Brünigstrasse 220, CH-6072 Sachseln, Switzerland*

Accepted 2018 September 4. Received 2018 July 18; in original form 2018 March 11

ABSTRACT

We describe here a novel design of a fast high-density robotized fiber positioner system for massive spectroscopic surveys. The fiber positioners are compact, robust, and they can be coordinated, allowing for a high spatial density. Furthermore, the high absolute accuracy removes the need for a metrology system and reduces the reconfiguration time. First, we present the requirements for such a high-density fiber positioner system and put them in relation with the science goals. Then, we discuss the positioner design that accomplishes these requirements (including mechanical design, local control electronics board, overall communication solution, and observation sequencing). Finally, the performance of the proposed design is measured using 25 mm pitch prototypes of the positioners, through a dedicated novel designed test-bench. The related results show that our prototypes fulfil the requirements particularly in terms of positioning precision (<20 μm rms for one single open loop move) and partially in tilt (<0.15 deg).

Key words: techniques: spectroscopic – telescopes – surveys – cosmology: observations – dark energy – large-scale structure of Universe.

1 INTRODUCTION

A new way of measuring the size of large-scale structures in the Universe and shedding light on the mystery of dark energy is the baryonic acoustic oscillation peak (Eisenstein et al. 2005). Key cosmological measurements of this baryonic acoustic oscillation peak in the distribution of galaxies (Anderson et al. 2012; Anderson et al. 2014) and in the Ly α forest of distant quasars (Delubac et al. 2015) have been achieved using the BOSS spectrograph on the Sloan Telescope (Sloan Digital Sky Survey – SDSS). These recent measurements and the prospects to have a clean method to probe the accelerated expansion of the Universe have steered the need to develop new massive spectroscopic instruments with a higher density of fibers and a shorter reconfiguration time. Indeed, the BOSS spectrograph is based on manual plugging of fibers in aluminium plates in the focal plane of the telescope, which takes several hours for the plugging but the plate design, manufacturing, and shipping is of the order of weeks. New projects which will be ready in the next few years, such as PFS (Prime Focus Spectrograph), MOONS (Multi-Object Optical and Nearinfrared Spectrograph), DESI (Dark Energy Spectroscopic Instrument), and 4MOST (4 m Multi-Object Spectroscopic Telescope) have been making rapid progress in this direction and will all use robotized positioning systems with 1000–5000 fibers. The main goal is to conduct spectroscopy on a large number of objects (1–50 million) over a wide field of view (from 0.15 to 7 square degrees) within a reasonable amount of time, thus opening new science opportunities for Galactic and Extragalactic spectroscopic surveys.

Before this new wave of projects, LAMOST (Large Sky Area Multi-Object fiber Spectroscopic Telescope; Xing et al. 1998), and the FMOS (Fiber Multi-Object Spectrograph; Kimura et al. 2010) were the first high-density robotized positioning systems to place all the fibers in a coordinated way at the targeted positions. However, these two systems initially suffered of some limitations due to lack of accuracy and long reconfiguration time, underlying the importance of the robustness, precision, and calibration of such complex systems.

Most of the new projects have adopted a SCARA-like RR planar kinematics (Makino & Furuya 1980) for the fiber positioning system, in particular: PFS with the COBRA fiber positioner (Fisher et al. 2009), DESI (Silber et al. 2012; Fahim et al. 2015), and MOONS (Cirasuolo et al. 2014). However, the 4MOST project has chosen the Echidna system de Jong et al. (2014).

This paper aims to highlight some of the guidelines to design fiber positioners for massive spectroscopic surveys. This is carried out through the presentation in detail of the design of our proposed fiber

★ E-mail: philipp.horler@gmail.com

positioner, the related issues and the performance results. The paper is structured as follows. Section 2 introduces the requirements for a robotized fiber positioning system and put them in relation to the scientific goals of the surveys. Section 3 presents the proposed design which fulfils these requirements (including mechanics, electronics, and software). Finally, Section 4 presents the measured performance using 10 prototypes, in particular the fiber-tilt and positioning accuracies and the absence of mechanical collision between adjacent positioners.

2 FROM ASTROPHYSICS TO MECHANICS

The purpose of the fiber positioner system (or *positioner* in short) is to place an optical fiber at a target position in the focal surface of the telescope, allowing the fiber to transmit the light from a particular object to a spectrograph. The thousands of fiber positioners are placed in a high-density pattern so that their workspaces overlap and fill the whole focal surface. This allows us to reach any point in the focal surface with at least one fiber but possibly more than one depending on the geometry of the positioner.

This section derives the requirements for a fiber positioner system from the science objectives of the astrophysical survey.

2.1 Science goals

The science goals of spectroscopic surveys are based on the parallel measurement of the light spectra of a large number of objects in a large field of view. The observed objects include stars, galaxies, and quasars of different magnitudes and the information extracted from their light spectra include redshift, relative velocities, and chemical composition but other information such as the imprint of the intergalactic medium in the line of sight of quasars can be collected. This information is used to better understand the history of our Universe and our Galaxy and to trace the formation of stars and galaxies.

The requirements to collect the light from a large number of objects means that the number of simultaneously measured objects (which is equal to the number of fibers) has to be maximized and the time between two measurements which is used to move the telescope and reposition the fibers to new targets has to be minimized.

2.1.1 Focal plane coverage

Any point in the focal plane should be reachable by at least one fiber (100 per cent coverage). This is the minimum to be able to observe any target in the field of view of the telescope. Sky background subtraction using $\sim$10 per cent of the fibers may be insufficient because (1) the sky background can vary a lot across a wide field of view (particularly at infrared wavelength) and (2) most targets are much fainter than the sky-background. We could increase the number of sky-fiber or in a more extreme case, we can arrange fibers in pairs: One fiber will be positioned on the target and the other one as close as possible next to it, thus allowing to measure the sky background close to the target. This means that any point in the focal plane has to be reached by at least two fibers as shown in Fig. 1, hence allowing a 200 per cent coverage.

The mechanical constraints of the positioner and particularly of the fiber holding part, should allow two fibers to be placed as close as possible to each other. If a machined part holding a ferrule is used, the minimum distance is typically a few millimeters in the focal plane (around one arcmin on sky). For tilting spines the minimum distance can be shorter as the fiber tips are only surrounded by the thin spine.

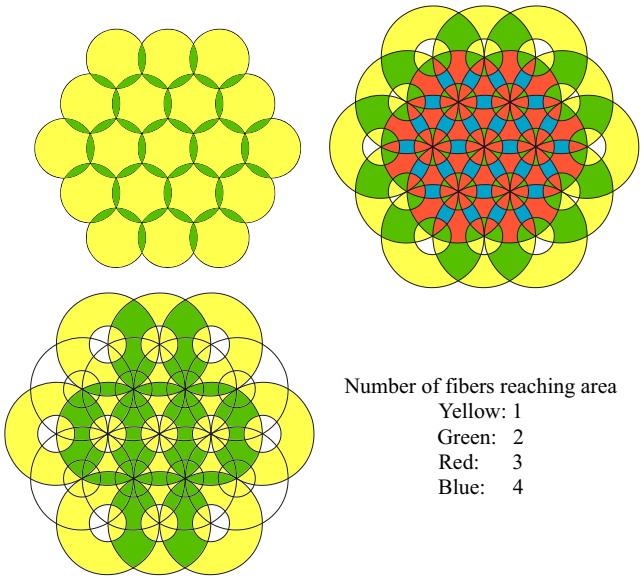

Figure 1. Single coverage (top left) and double coverage (top right) of the focal surface. Bottom left shows the coverage using the double coverage geometry, but using only half of the positioners.

In some cases, when the survey uses multiple spectrographs (for e.g. a visible and an IR spectrograph), one fiber positioner could hold more than one fiber. If the spectrographs do not accept the same number of fibers, there will be part of the positioners carrying both types of fibers and another part of the positioners carrying only one type of fiber. In that case it is preferable to have at least a 200 per cent coverage, such that we still have a 100 per cent coverage using only half the positioners.

In the case of a SCARA-like kinematics (cf Section 3), the arm lengths have to be chosen. We can distinguish two approaches

(i) *Single coverage*: In this approach, both arms of the positioner have the same length, allowing it to reach its own centre. The workspaces are full circles which overlap just enough to cover the whole surface. Thus, most of the surface is covered by a single fiber as shown in Fig. 1 (top left).

(ii) *Double coverage*: In this approach, the beta arm is longer than the alpha arm (see Fig. 5). The positioner cannot reach its own centre and the circular workspace has a hole in the centre. To cover the whole focal surface, the arms have to be long enough to reach the centre of the adjacent positioners. The resulting overlap guarantees at least a double coverage of the whole plane as shown in Fig. 1 (top right).

In the case of the double coverage, the exact ratio between the arm lengths has to be chosen. For a maximum coverage we want to minimize the ratio i.e. minimize the hole in the workspace. The limit is given by the condition of no mechanical collision between positioners. If the alpha arm is too long, it will collide with the alpha arm of the adjacent positioner. The maximum length of the alpha arm is half the pitch, minus the physical envelope of the guidance and actuator of the beta axis. The advantage of the double coverage is that nearly 100 per cent of the focal surface is covered using only half of the positioners.

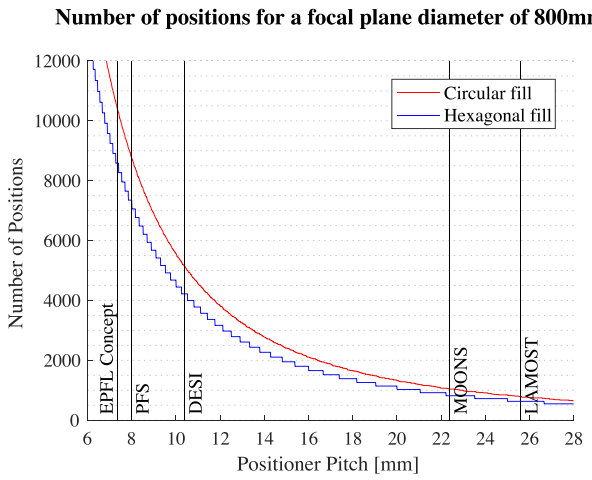

Figure 2. Number of positioners in function of the pitch. The red line is obtained filling the whole circular focal surface. The blue line is obtained filling only a hexagonal shaped area within the circular focal surface. The pitches of some projects are shown for reference.

2.1.2 *Density of positioners/pitch*

The pitch between fiber positioners and therefore the spatial density of positioners is given by the focal surface area and the number of positioners. A rough relation between the pitch p, the focal surface area $A_{\mathrm{foc},}$ and the number of positioners N_{pos}, is given in equation (1)

$$p = \sqrt{\frac{2}{\sqrt{3}}\frac{A_{\mathrm{foc}}}{N_{\mathrm{pos}}}} \qquad N_{\mathrm{pos}} = \frac{2}{\sqrt{3}}\frac{A_{\mathrm{foc}}}{p^2} \tag{1}$$

For an exact calculation of the number of positioners, some more details have to be taken into account: In addition to the fiber positioners, guidance cameras, and metrology fiducials will have to be placed in the focal surface. One approach is to fill only a hexagonal shaped area within the circular focal surface, which leaves six wedges on the periphery for such devices. Fig. 2 plots the number of positions (which can be filled by either a positioner or a fiducial) in function of the pitch for a circular focal surface of 800 mm in diameter.

The focal surface area is a quantity defined by the existing telescope for which a new instrument is being designed. If a new telescope is to be built, or if an existing telescope can be modified (e.g. to allow a wider field of view), the focal surface should be maximized to facilitate the design of the fiber positioners. However, the ratio between the focal surface diameter and the field-of-view diameter of the telescope has to be designed such that the size of the observed objects matches the size of the fiber cores. For a given ratio, for e.g. 100 μm arcsec^{-1}, the focal surface area is proportional to the field of view of the telescope. A way to overcome this constraint is to add microlenses in front of each fiber as described in Section 2.1.3.

The number of positioners on the other hand is mainly driven by the number of fibers the spectrograph can accept, which in turn is driven by the science case (usually the goal is to have as many as possible) and limited by the budget (the detectors of the spectrograph are generally the most expensive part of such an instrument).

2.1.3 *Size of fibre cores*

In most cases the fibre tips are located in the focal plane and an image of the observed objects is projected onto the fibre core. The fibre core acts as a field stop and defines the light collecting area. Its size should match the typical size of objects (convoluted by the typical seeing size of the telescope site). Point objects and far galaxies are smaller than the typical seeing of 0.5−1 arcsec at most telescope sites. The typical plate scale of astronomical telescopes is 50−100 μm arcsec^{-1} so the fibre core size of a multimode fibre of 100−150 μm covers all objects.

In some cases the plate scale is bigger and a bare fibre would be too small. In that case one can add a microlens in front of each fiber. The microlens has to be placed in the focal plane and projects the light onto the smaller fiber core, changing the *f*-ratio. The cost is an increased complexity of the fiber assembly and an additional source of error (misalignment of the microlens with respect to the fiber) and throughput loss.

2.1.4 *Stray light*

Incident light of bright objects which are not observed can potentially be reflected by any surface on the positioners and end up in the fibers observing fainter objects. Therefore, any part of the positioners exposed to incident light should absorb as much light as possible to avoid stray light. This concerns all parts which are located between the focal plane and the support plate and are exposed to incident light. Their surfaces should be treated to maximize absorption (for e.g. black anodizing) and if possible inclined with respect to the focal surface. It is also possible to add a light-trapping blind hole on the beta arm of a positioner. In this way the light of an extremely bright star can be trapped in the blind hole of one dedicated positioner.

2.1.5 *Lifetime and reconfiguration time*

The lifetime of the instrument is driven by the scientific goals of the survey, for e.g. 10^6 measurements over 10 yr. The available time on the telescope should be used efficiently for exposures and the time between two exposures has to be kept as short as possible. The time between two exposures is used to readout the detectors, slew the telescope and reconfigure the fibers for a new field. The reconfiguration time of the fiber positioners should not be longer than the readout and slew time, typically in the order of 60 s.

The usage of the positioners is very sporadic. The positioners are only moved during reconfiguration between two exposures. In order to ensure such lifetime given the usage, the actuators have to be designed with suitable characteristics regarding lubrication and preload.

2.2 Instrument efficiency

This subsection lists all requirements which aim to reduce loss of light between the telescope and the spectrograph.

2.2.1 *XY accuracy*

A positioning error of the fiber in the *XY* plane induces loss of light by vignetting. On one hand some of the light of the object will not fall onto the fibre core, and on the other hand more sky background will be collected. The tolerance on the XY positioning error is therefore proportional to the fiber core diameter. Small, seeing-limited objects have a projected image smaller than the fiber core and a XY Error of a few per cent of the core diameter is acceptable. Typically the XY tolerance is ∼4 per cent of the core

diameter (∼5 μm for a 125 μm fiber core in DESI and ∼20 μm for a 600 μm microlens in MOONS). For more extended objects, for which the image is bigger than the fiber core, the throughput loss depends on the intensity profile, but is smaller and a larger tolerance is generally acceptable.

2.2.2 *Z accuracy*

An error in the *Z*-direction moves the fiber out of focus which will result again in light loss as the projected image of the object gets bigger than the pupil. The relative increase of the diameter d depends on the error in the *Z*-direction Δz, the f number of the light f and the diameter itself

$$\frac{\Delta d}{d} = \frac{\Delta z}{df}. \tag{2}$$

The exact amount of light loss however depends on the brightness distribution across the object itself. A typical Z tolerance for a 125 μm fiber and an f number of four is ∼50 μm.

2.2.3 *Tilt accuracy*

The fiber tip (and microlens assembly if applicable) has to be aligned with the chief ray, perpendicular to the focal surface. Any tilt error will induce focal ratio degradation in the fiber which will finally cause throughput loss as the light coming out of the fiber at the other end will exit with a bigger angle. The requirement for the tilt error depends on the f number of the telescope, the fiber, and how the spectrograph is designed. Usually the acceptance angle of the fibre is slightly bigger than the light cone coming from the telescope and the collimator in the spectrograph accepts a fiber output beam a bit faster than the nominal one. Both of these measures increase the acceptable tilt error. As an e.g., an error of 0.2° on a *f*/4 beam will decrease the f number to 3.89. In these cases the tolerance on the tilt of the fiber is typically a few tens of degrees.

In some cases however, the f number of the telescope is smaller than the one accepted by the fibre. For e.g. the primary focus of the Subaru telescope is *f*/2. In these cases the fiber has a bigger f number and acts as an aperture stop. A tilt error has no effect until the light cone accepted by the fiber exits the light cone coming from the telescope. For e.g. a fiber accepting a *f*/3.6 beam on a *f*/2 telescope, can have a tilt error of up to 6.1° without throughput loss.

2.2.4 *FRD due to fiber stress*

Another source of light loss lies within the fiber. Mechanical stress degrades the focal ratio in the fiber. The fiber path has to be chosen in a way to minimize stress in the fiber. In general we can say that bending, torsional stress, and contact with sharp edges has to be avoided. However, it is not obvious to define a requirement on fiber stress for the mechanical design. A solution is to define a minimum bending radius of the fiber (for e.g. 50 mm), which can be estimated using Ramseys formula (Ramsey 1988) or has to be determined experimentally on test fibers.

$$\frac{\Delta\Theta}{\Theta} = \frac{d}{R} \tag{3}$$

Θ is the angle of the incident light with respect to the fiber axis, $\Delta\Theta$ is the radial dispersion, d is the core diameter, and R is the bending radius. An illustration is shown in Fig. 3.

Torsional stress has also to be considered, specially in the case of SCARA kinematics. In such designs, the fiber should not be constrained on the positioner, such that a rotation of the fiber tip is distributed over a bigger length, ideally until they are bundled. In that case FRD due to torsion can be constrained. Again, this has to be verified experimentally, specially for large fiber diameters.

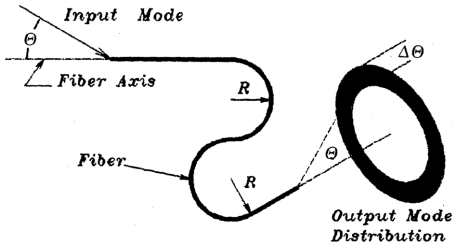

Figure 3. Illustration of FRD.

Another solution is to define a maximum throughput loss due to fiber stress (for e.g. 0.5 per cent). This number can only be verified on a prototype positioner with a test fiber, whereas a minimum bending radius can be taken into account during the design phase of the positioner.

As said in Section 2.2.3, the spectrograph design usually has a built in tolerance for FRD by accepting a slightly faster beam than the nominal one. The tolerance on the FRD of the fiber depends therefore also on the spectrograph design.

2.2.5 *Difference in focal ratio between fiber input and output*

Except for the FRD described above, the focal ratio at the output of the fiber is equal to the focal ratio at the input of the fiber. In order to maximize the throughput of the fiber, the input and output focal ratio should correspond to the nominal numerical aperture (NA) of the fiber. The focal ratio of the telescope can be corrected for the fibers using a field corrector (one for the whole field) or microlenses (one per fiber), both of which introduce additional throughput loss due to absorption and misalignments. If a new telescope is being designed, the focal ratio of the telescope should be designed to match the NA of the fibers.

In the example of the DESI instrument, the telescope projects light at *f*/4 and the spectrograph can accept light at *f*/3.57.

In the example of the MOONS instrument, the focal ratio of the telescope and field corrector is *f*/15. The focal ratio at the output of the fibers in the spectrograph is *f*/3.5. The microlenses project the light at *f*/3.65 onto the fiber core. In this way, the transmission loss due to the focal ratio difference is less than 2.5 per cent.

2.3 Telescope constraints

2.3.1 *Operational temperature and humidity*

As the fiber positioners are placed in the focal plane of the telescope, they are typically located in the dome of the telescope. This means that the operating temperature has to be kept within few degrees Celsius of the ambient night temperature in the dome. In the case of the Mayall (DESI), VLT (MOONS), and Apache Point (SLOAN) this temperature varies between −10°C and 30°C.

Similarly, for good seeing conditions, the humidity has to be very low at the site of the telescope. These factors are to be taken into account in the mechanical design when choosing the lubricant of the ball bearings and the gearbox and glue, if any.

2.3.2 Heat dissipation

The *average* power consumption of the positioners is limited by thermal considerations: If the positioner dissipates too much heat toward the focal plate and the environment, thermal expansion will introduce *XY* errors to the fibers and worse, create turbulences in the dome and disturb the seeing of the telescope. As the positioner is idling the majority of the time, the actuators are not powered while idling, and the local drive electronics are turned off or put into low power sleep mode. In that way, the average heat dissipation can be kept very low. *This means that the positioners have to keep the position of the fibers passively during the observations.* In the case of motors and gearheads, this is an argument in favour of irreversible gearheads which makes them hold the position passively.

The *maximum* power consumption in the active state is mainly limited by the electrical current supply to the focal plate. In the case of the DESI instrument, each positioner typically consumes several hundred mA at 5–10 V. If we consider 5000 positioners, the whole focal plate needs over 1 kA at 5–10 V. The high current requires a special power supply and very bulky and heavy electrical connections between the power supply and the focal plate.

2.3.3 Earthquake resistance

In the case of the VLT, the telescope is located in an earthquake active area. There is a very high probability that an instrument will have to resist a strong earthquake within its lifetime. Therefore the mass of the positioner is critical for the structural integrity of the instrument. In the case of the MOONS instrument, structural simulations suggest a limit of 200 g per positioner.

2.3.4 Collision avoidance

The possibility for pairwise observation of targets (one fiber on the target and one next to it for background subtraction) requires overlapping workspaces, which creates a risk for collisions between adjacent positioners. A decentralized path generation algorithm is necessary to guarantee collision-free trajectories for all positioners in a practical amount of time (Makarem et al. 2014).

2.4 Summary

A summary of this section is presented in Table 1. The needs of the surveys are shown with the corresponding requirements and a numerical example taken from the MOONS instrument.

3 FIBER POSITIONER DESIGN

The design proposed here is based on the requirements of the MOONS instrument. However, it is generic in the sense that it can be adapted to suit the requirement of most known projects (cf. Section 1) and hopefully future projects. However, it may not be the optimal design choice for a given project if the requirements are very different. For e.g. a larger tilt tolerance or if a metrology system is available.

3.1 Mechanical design

The kinematics of the positioner presented in this paper is a SCARA-like planar configuration with two rotational degrees of freedom. It allows the movement of the optical fiber in the X and Y directions. An overview of the positioner is shown in Fig. 4. The two axes, α and β, are nearly parallel (cf Section 3.1.1). α is in the centre of the workspace and β is 8 mm eccentric as shown in Fig. 5. The first arm is 8 mm long and the second arm is 17 mm long. The workspace of the positioner has annular shape with an outer diameter of 25 mm and an inner diameter of 9 mm. Both axes have a motion range of more than 360° in order to reach any position in the workspace in left- or right-handed configuration. Mechanical hardstops are implemented to prevent winding up of the fiber. Fig. 6 shows the hardstop on the alpha axis. The floating green part is necessary to achieve a motion range of more than 360°. The alpha axis has a hollow shaft for the fiber to go through. As opposed to having the fiber outside the positioner, this minimizes the bending of the fiber and removes any risk of neighbouring fibers colliding. Unfortunately, there is no standard hollow shaft motor-gearhead combination available in this size. To overcome this, the lollipop feature is implemented. It transmits the rotation of the actuator to the hollow shaft via just one radial connection. This allows the fiber to pass from the hollow shaft to the side of the actuator.

3.1.1 Tilt of the axes

The ferrule has always to be aligned with the chief ray of the light that it captures. The focal surface of this light, defined by the telescope and the corrector optics, can be approximated by a sphere with a radius of ∼4 m and is concave towards M3. To account for this curvature, the physical focal plate is curved and neighbouring positioners are tilted by 0.35° to each other. This is more than twice the tolerance on the tilt error. Therefore, this curvature has to be accounted for even within the workspace of a positioner. While the alpha axis is perpendicular to the focal plate, the beta axis is tilted to the alpha axis by 0.11° and the ferrule is tilted to the beta axis by 0.24°. These angles are illustrated in Fig. 7. By tilting the beta axis and the ferrule, the ferrule will always follow the focal surface and be aligned with the chief ray.

3.1.2 Alignment of the axes

The alignment of the two rotation axes is the most critical part of the mechanical design. As the tilt error of the ferrule will be a sum of manufacturing tolerances on all parts and interface errors between all parts between the focal plate and the ferrule, the number of parts is kept at a minimum. Both axes are defined by two widely spaced and preloaded ball bearings. The axial preload is achieved by compressing an elastic spring washer which is mounted with the bearings and a spacer. A nut secures this assembly. It is locked against a hardstop and the compression of the spring washer is defined by the dimensions of the parts for simple assembly. An illustration is given in Figs 8 and 9. The interfaces on the parts which are critical for the alignment are machined as the last operations on the part and in the same take to minimize machining errors.

3.1.3 Flexible coupling

Both rotation axes are well defined by two preloaded bearings. If the motors were connected directly to the axes, the additional bearing of the gearhead output would over constrain the axes and the alignment precision would be deteriorated. The solution is to use a flexible coupling which is compliant for tilt, radial, and axial misalignments between the gearheads and the axes. The chosen variant is a bellow coupling, which is stiff in torsion and has no backlash.

Table 1. Example of fiber positioning requirements, taken from the MOONS instrument.

Need	Requirement	Value
Pairwise observation	Focal plane coverage	Each position reachable by at least 2 positioners
Pairwise observation	Minimal fiber distance	4 mm
Telescope field of view and science goal	Pitch	25 mm
Target size	Size of the pupil	610 μm
Survey length	Lifetime	10^6 Movements/10 yr
Science goal	Reconfiguration time	<30 s
Instrument efficiency	rms *XY* error	<20 μm
Instrument efficiency	*Z* max defocus error	<50 μm
Instrument efficiency	Max tilt error	±0.15°
Instrument efficiency	FRD due to fiber stress	<0.5% throughput loss
Instrument efficiency	Difference in focal ratio between fiber input and output	<1%
Environment temperature	Operational temperature	−10°C to +30°C
Environment humidity	Operational humidity	5%–20%
Low heat dissipation	Power while active	<2 W
Low heat dissipation	Power while inactive	0 W
Earthquake resistance	Mass of the positioner	<200 g

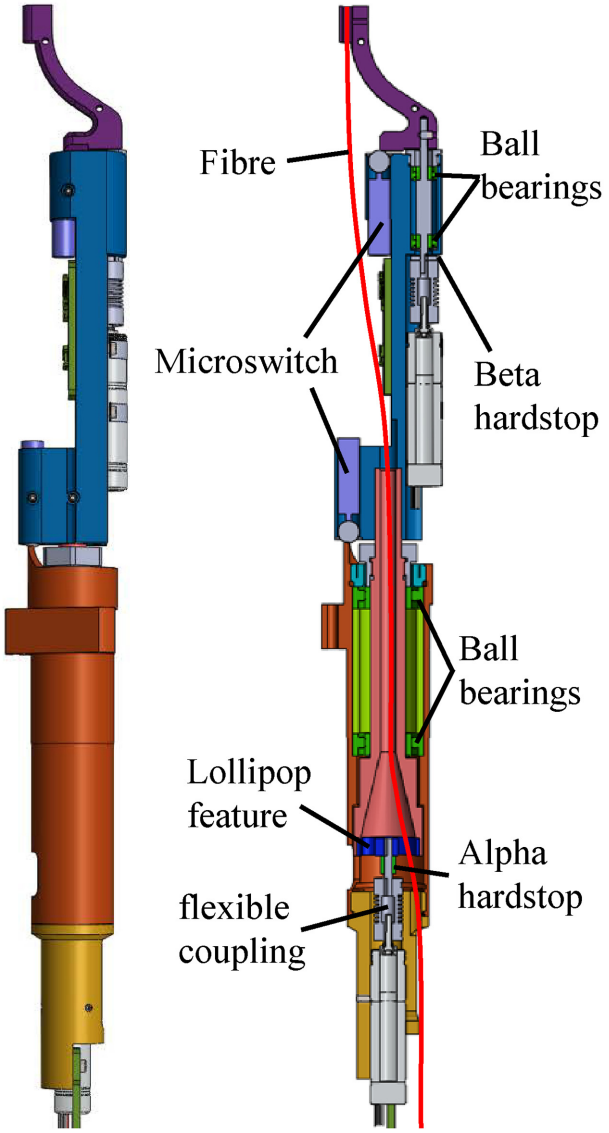

Figure 4. Cut view of the positioner. The path of the fiber is shown in red.

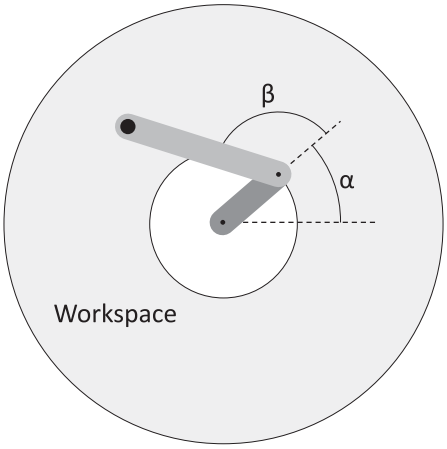

Figure 5. Cinematic and workspace of the positioner.

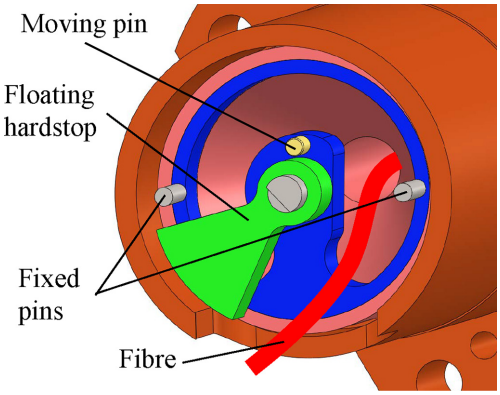

Figure 6. Cut view of the positioner revealing the hardstop of the alpha axis and the lollipop feature.

3.1.4 Micro switches

Each axis is equipped with a micro switch which gives it an absolute reference position. With these micro switches, the positioner can recalibrate itself without the need of an external calibration system. The switches have a diameter of 5 mm and an actuation repeatability

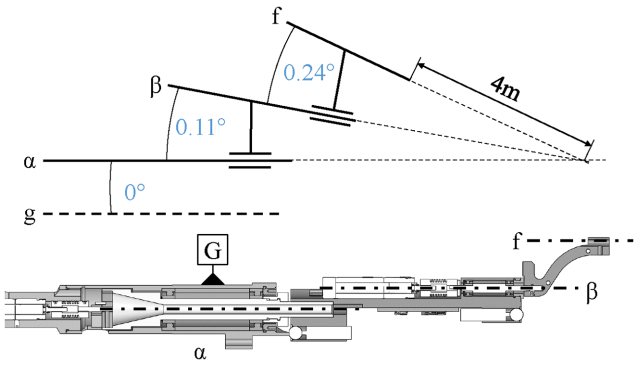

Figure 7. Tilt definitions.

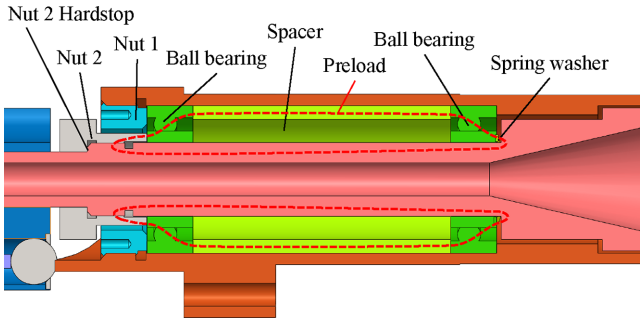

Figure 8. Preload of the alpha axis bearings. Nut 1 secures the spacer and the outer rings of the bearings to the chassis. Nut 2 is locked against a hardstop on the hollow shaft and creates the preload via the inner rings of the bearings and the spring washer.

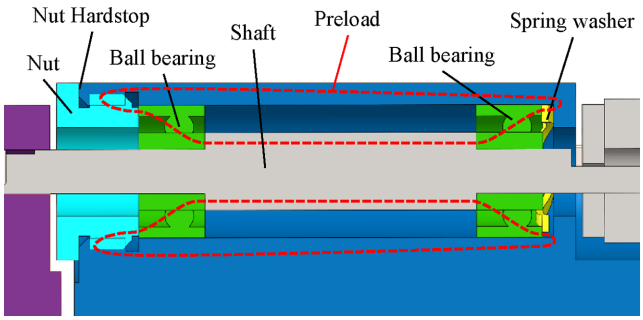

Figure 9. Preload of the beta axis bearings. The nut is locked against a hardstop on the housing and creates the preload via the inner rings of the bearings and the spring washer.

of 1 µm. The rotational movement is converted into a translational movement via an inclined surface and a transfer ball. Figs 10 and 11 show the implementation of the switches. Both switches are fixed to the alpha arm (rotate with the alpha axis) and make contact to the base of the positioner and the beta arm.

The motion range of both axes is more than 360° which allows the micro switches to be placed near both ends of the motion range. In this way they can be used as soft stop before the hard stop. This can be useful to prevent hitting the hard stop in case of wrong motor commands. On the other hand it is also useful to place the micro switch in the middle of the motion range. Especially if an absolute recalibration is necessary between each repositioning. In addition, a calibration position with collision potential is to be avoided in the case of the beta axis.

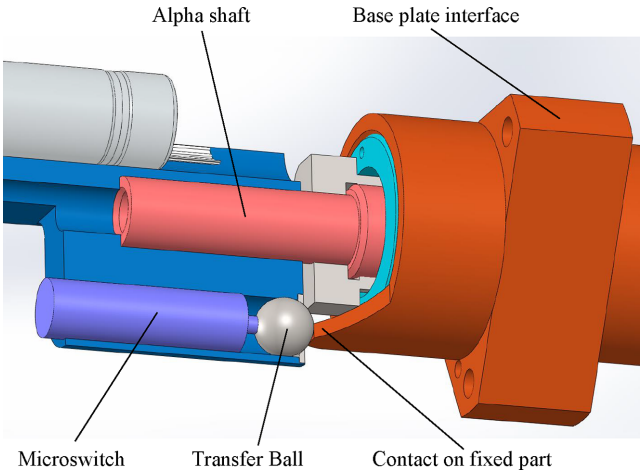

Figure 10. Partial cut view of the alpha switch implementation.

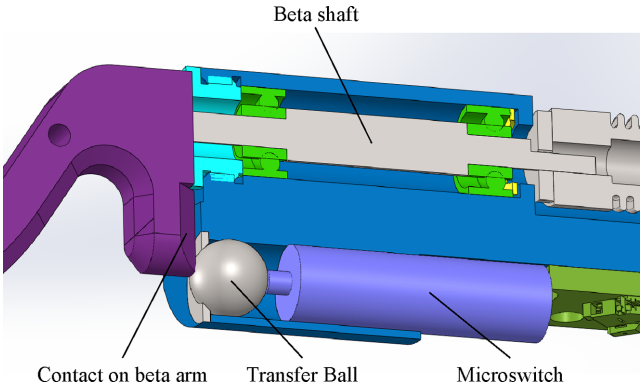

Figure 11. Partial cut view of the beta switch implementation.

3.1.5 Reduction Ratio

The chosen reduction ratio of the gearhead is 650:1. There are several reasons for this high value:

(i) A high ratio increases the positioning resolution. Whether a sensor is used on the motor side or an open loop solution is chosen, in any case, the positioning resolution is multiplied by the reduction ratio. (The precision however will be limited by backlash and non-linearities in the gearbox).

(ii) The chosen gearheads are backlash reduced gearheads where two spurgear trains are preloaded against each other. The preload can be made more precisely, the more stages there are. Therefore, the backlash will be reduced best with a high reduction ratio.

(iii) A high gear ratio makes the reduction gears not back drivable and the gearhead will provide the holding torque passively when the power is turned off.

3.1.6 Actuators

The chosen actuators are brushless DC motors in combination with high ratio, backlash reduced planetary gearheads. Another possible choice would be stepper motors. Brushed DC motors are not considered because their performance is affected by wear within the required lifetime. This section discusses the choice between brushless DC and stepper motors.

Apart from the variable reluctance type stepper motor, which is difficult to downscale, stepper motors have the characteristic of

Figure 12. Picture of the integrated drive electronic.

having a passive holding torque. The consequence is that when the power is turned off, they can only stop at a full step. This requires a very high reduction ratio, for e.g. a ratio of at least 500:1 is needed for a motor with 20 steps per turn. It is a common misconception that the passive holding torque helps the positioner to keep its position during the exposure of the telescope: The high ratio gearheads are not backdrivable, and provide by themselves the needed passive holding torque.

An advantage of the stepper motor is the higher pole number. Typically a stepper motor has 20 poles whereas a brushless DC motor typically has only one. This increases inherently the positioning accuracy. For both motor types, a vectorial control can be applied to increase the resolution. However, the passive holding torque of the stepper motor will limit the resolution to the number of steps.

A disadvantage of the stepper motor is that it needs four wires while a brushless DC only needs three. The reduced number of wires which share the hollow shaft with the fiber reduces contact and stress on the fiber.

In the case of this fiber positioner, a brushless DC motor is chosen because in this size (⌀8 mm) there is no variable reluctance stepper motor available. In addition brushless DC motors are more suitable for a future downscaling of the design due to their simpler construction. Currently, the smallest of-the-shelf stepper motor is ⌀6 mm (ref Faulhaber), while the smallest brushless DC is ⌀4 mm (ref Faulhaber, Maxon, Namiki), and ⌀2 mm prototypes are already available (ref Namiki).

3.2 Drive electronics and software

Each positioner has its own local electronic board. The task of this board is to control both motors, read sensors, and communicate with a central unit. The board is attached at the back of the positioner and has to fit into the space envelope of the positioner. As the positioner and electronic board become a single unit, the number of wires connecting each positioner to the central unit is kept to a minimum. The processing unit of the board is a STM32F405 micro controller. It features a CAN interface for the communication, timers for PWM signal generation, GPIO pins and ADCs to read out sensors and enough memory to store trajectories. A picture of the prototype board is shown in Fig. 12.

3.2.1 Communication

The central unit has to send various commands (status requests, motor control parameters, Request to go to datum) and trajectories for both motors. The micro controller has to answer to status requests, notify when movements are completed and send error reports.

The communication with the central unit is realized using a CAN bus. Multiple positioners share a common bus and the central unit can send individually addressed messages or broadcast messages to all positioners on the bus. A CAN bus for the 10 prototype positioners has been realized and tested. For the case of 1000 or more positioners, multiple CAN busses have to be implemented because the CAN bus is physically limited to ∼150 devices. A solution using four embedded PCs as intermediate layer is proposed

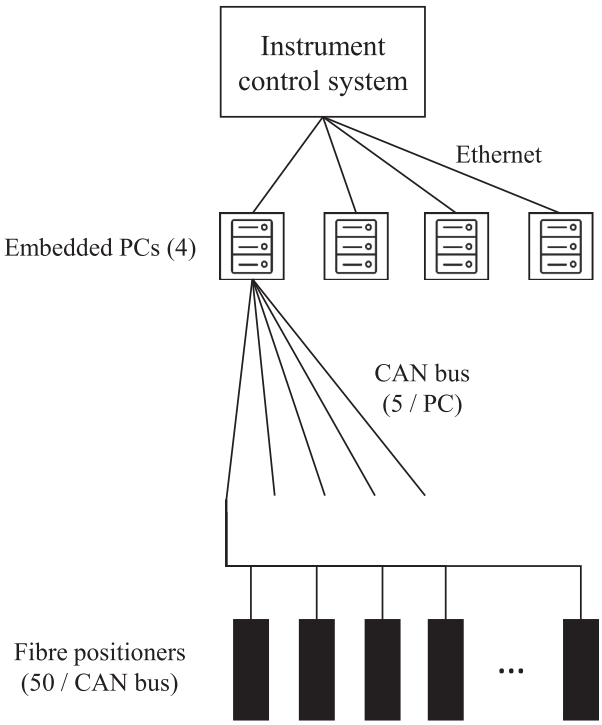

Figure 13. Proposed architecture for the communication with 1000 positioners.

in Fig. 13. Each embedded PC communicates with the central unit via Ethernet and manages five CAN busses with 50 positioners on each CAN bus. The number of Embedded PCs in the intermediate layer and the number of CAN busses per Embedded PC can easily be increased for a larger number of positioners.

3.2.2 Trajectory interpolation

The two trajectories sent via CAN bus consist of a set of points $p_i = (t_i, \theta_i)$, where t_i are the time coordinates and θ_i the angle coordinates. The micro controller interpolates linearly between those points to create a trajectory with constant velocity segments. The simplest trajectory, a constant velocity until the target, consists of only one final point; only two 32bit numbers. If there is a need to ramp-up to higher velocities and/or manoeuvres for collision avoidance, the trajectory can be made of any number of points (the RAM memory of the micro controller can store several thousand points). However, keeping the number of points low reduces the required time to send the trajectories to the positioners.

3.2.3 Motion control

An open or closed loop control strategy can be used to drive the motors. In both cases a vector control is used on the stator coils to set the angle of the magnetic field. In the case of an open loop control, the angle of the magnetic field is set to the angle of the trajectory. The current is set to a fixed value. In case of a closed loop control, the magnetic field is set to $\pm 90^\circ$ with respect to the angle of the rotor to maximize its efficiency. The applied current is proportional to the torque and is the output of a PID position controller. The closed loop control is inherently more energy efficient.

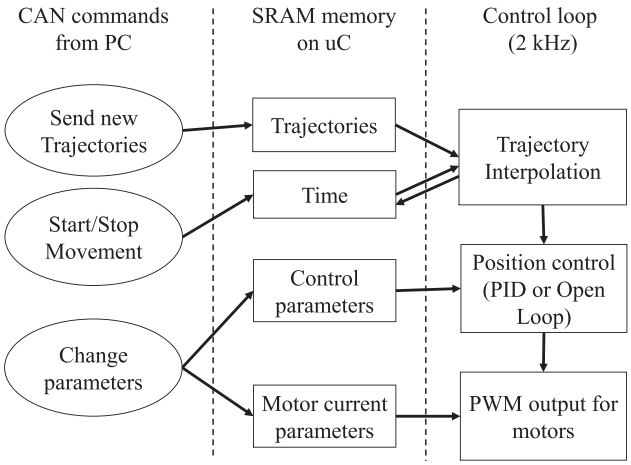

Figure 14. Block diagram of the code executed in the micro controller.

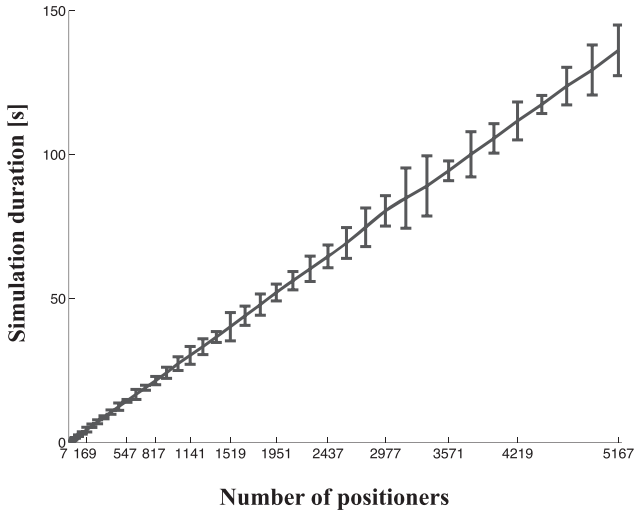

Figure 15. Collision avoidance algorithm execution times in function of the number of positioners. The errorbars are 10 times the standard deviations. Figure taken from (Makarem 2015).

The trajectory interpolation and control loop are run at 2 kHz. A block diagram of the code in the micro controller is given in Fig. 14.

3.2.4 Observation sequence

A typical observation block consists of a 10 min to 1 h exposure in a certain area of the sky. During the exposure, the position of the fibers has to be kept and the power of the positioners is shut down. Each observation block is prepared in advance by selecting the targets, assigning them to positioners and generating the trajectories using the collision avoidance algorithm. Due to changing weather conditions, observation blocks have to be interchangeable. Therefore each block starts and ends with the positioners in the home position. In the case of the MOONS positioner – using an arm ratio for double coverage – the collision avoidance algorithm is quite complex and has to be executed offline. Fig. 15 shows the execution times in function of the number of positioners. For an instrument with a small number of positioners or a positioner kinematics allowing for simpler collision avoidance algorithms, one can

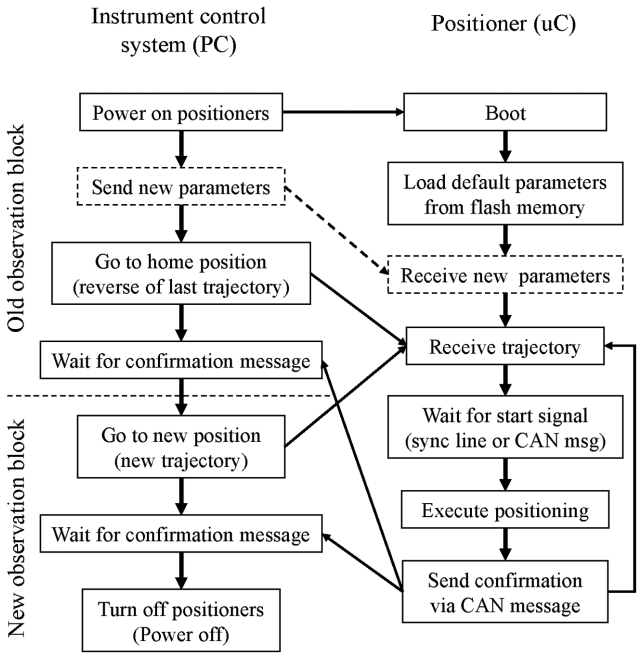

Figure 16. Typical operation sequence between two observation blocks.

run the collision avoidance online and doesn't have to go to a home position between observation blocks.

Fig. 16 shows the typical operation sequence between two operation blocks on the instrument control system and the positioner electronic board.

3.2.5 Bootloader

Flashing code to the micro controller requires a jTag or a serial connection from a PC and cannot be done via CAN bus inherently. If for some reason the code has to be updated, the positioners have to be removed from the focal plate in order to access the electronics board. This is a complex operation requiring several weeks of downtime. Therefore a bootloader allowing to reprogram the micro controller via the CAN bus has been implemented. Initially only the bootloader will be flashed from the PC. It is a program which boots on the micro controller and communicates to a central unit via CAN bus. The central unit can send a new executable code which the bootloader will write to the flash memory of the micro controller. The bootloader then starts the main program. This allows reprogramming of all positioners without physical intervention.

4 PROTOTYPE PERFORMANCE

In order to evaluate the performance of the presented design, 10 prototypes have been built according to the mechanical design presented in Section 3.1 and using the drive electronics presented in Section 3.2. The actuators used are 8 mm brushless motors with backlash free reduction gears (preloaded double spur gear train) with a ratio of 650:1.

4.1 Test methods

Two test setups have been used for the evaluation of performance.

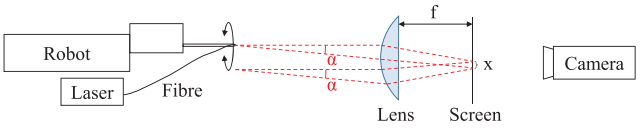

Figure 17. Tilt bench principle. The tilt of the ferrule can be calculated by measuring x.

4.1.1 Positioning bench

The first setup measures the *XY* position of the fiber using a backlit multimode fiber and a camera in front of the positioner. The absolute *X*/*Y* accuracy of this setup is of 1 μm.

4.1.2 Tilt bench

The second setup is an optical bench which allows simultaneous measurement of the position of the fiber and its tilt anywhere in the workspace. A backlit single mode fiber emits a cone of light through a lens on a screen located at the focal length of the lens. In this way, the position of the light on the screen gives the tilt of the fiber independently of the position of the fiber as shown in Fig. 17. The tilt α of the fiber is given by

$$\alpha = arctan\frac{x}{f}, \tag{4}$$

where x is the displacement on the screen (in two dimensions) and f the focal length of the lens. A second camera measures the position by seeing the fiber directly without using the screen. The *XY* position precision is of 10 μm and the tilt precision is of 0.01°.

4.2 Calibration

The position and tilt measurements are used to calibrate the prototypes. The rigid body model of the positioner is a 2 degrees of freedom SCARA kinematics with slightly tilted axes. The calibrated parameters are:

(i) Location of alpha axis (centre of positioner).
(ii) Alpha and beta arm length.
(iii) Angular position of alpha and beta micro switch.
(iv) Tilt of the alpha axis with respect to the base plate.
(v) Tilt of the beta axis with respect to the alpha axis.
(vi) Tilt of the ferrule with respect to the beta axis.
(vii) Non-linearity of the gearmotors.

Fig. 18 shows an example of the measured non-linearity of one gear transmission. The non-linearity is the deviation from a linear, constant ratio gear transmission. It is measured by commanding the positioner to do a full rotation and measuring the movement of the positioner using the test bench. Measurements are taken at 4000 positions evenly spaced around the revolution. As it can be seen in Fig. 18, the effect of the non-linearity of the gear transmission on the fiber position (∼300 μm) is an order of magnitude larger than the precision requirement. However, it is repeatable to 1.5 μm and can therefore be calibrated for. A Fourier transform of the non-linearity shows that over 200 measurements per revolution, the amplitude remains under 1 μm. Therefore the calibration can be done with 200 points per actuator. It is important to limit the number of points because each positioner has to be calibrated individually.

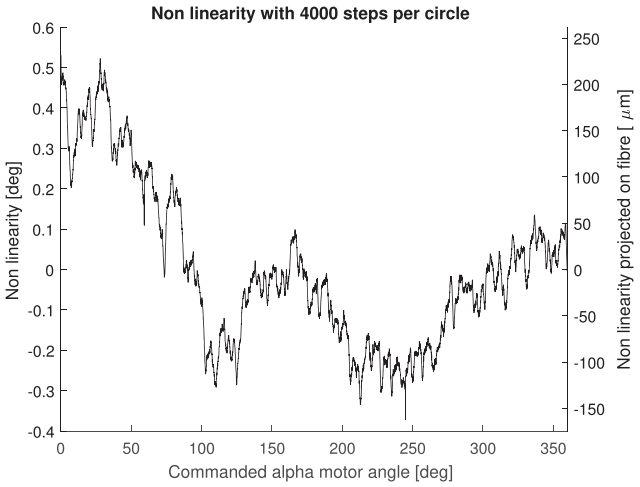

Figure 18. Non-linearity of the transmission measuring 20 (top) or 4000 (bottom) steps on the circle.

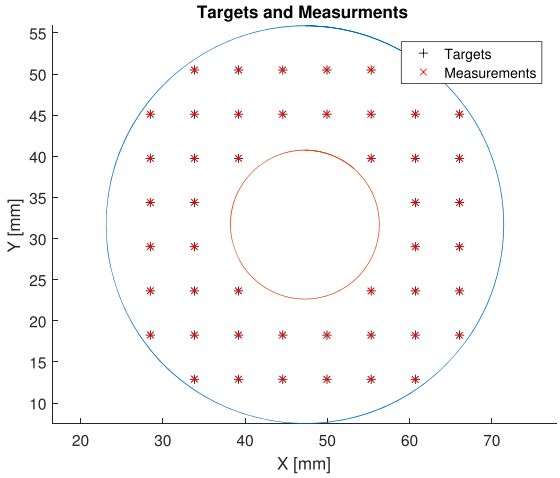

Figure 19. Grid of test targets and corresponding measurements.

4.3 Positioning performance

4.3.1 Accuracy

The calibration parameters described in Section 4.2 including the non-linearity are used to generate motor commands for a grid of test targets as illustrated in Fig. 19. For each positioner, the rms of the absolute error is shown in Fig. 20 (top). Positioners 6 and 9 are missing because their reduction gears were damaged and the preload for the backlash reduction is missing. Five of the remaining eight fulfil the *XY* accuracy requirement and the average error is 20 μm with a standard deviation of 3.9 μm.

4.3.2 Repeatability

Each point of the tilt measurement procedure is visited multiple times by the positioner and therefore the repeatability in positioning can be measured on each of these points. Fig. 20 (bottom) shows the repeatability of all positioners. Note that most positioners are repeatable to the precision of the test bench.

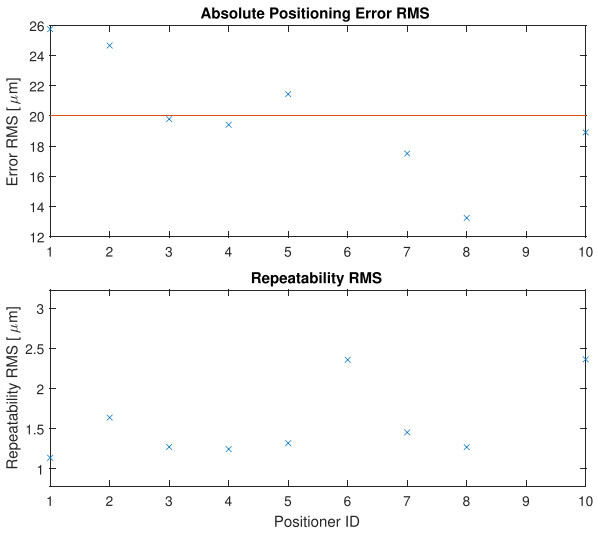

Figure 20. Absolute accuracy of positioning and repeatability for the 10 prototypes.

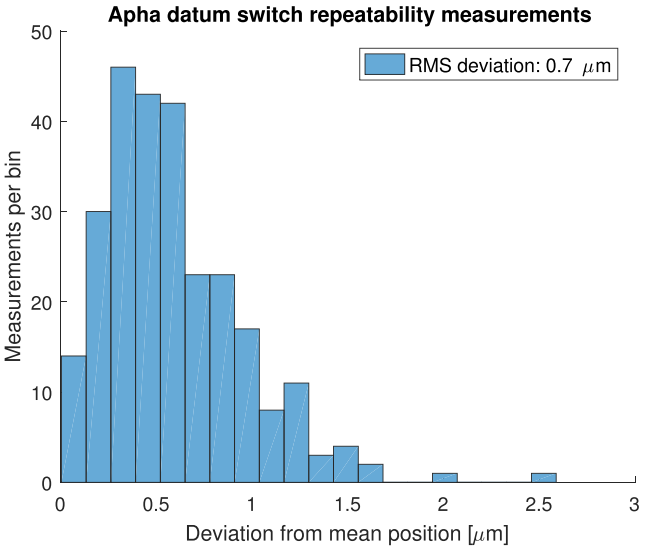

Figure 21. Datum switch repeatability.

4.3.3 Hysteresis

The hysteresis of each axis is measured by approaching all points of the calibration procedure from either side. The difference in position of the measurements is then converted into an angle on the actuator axis. Similar to the non-linearity, each transmission has a different hysteresis curve within the revolution. The average of all motors is 0.039° with a standard deviation of 0.035°.

It can be observed that with an arm length of 25 mm, a hysteresis of 0.039° translates to an error of 17 μm; however, the maximum values are around 60 μm. This is three times the required accuracy. Therefore, even with the backlash reduced gearheads, it is still necessary to approach the targets always from the same side. Thanks to the still relatively low hysteresis, this can be done by an additional back and forth movement at the end of the generated trajectory, without the need of running the collision avoidance algorithm again.

4.3.4 Datum switch repeatability

The Datum switches are an absolute reference for the positioner. By running against the switches, it is able to recalibrate its position in case some steps were lost during observation or after a power failure. The precision of subsequent positioning depends (among other factors) on the precision of this switch. The precision of the alpha switch has been measured by repeatedly running the positioner against the switch and recording its position each time. The histogram of the deviation from the mean position is shown in Fig. 21. The rms value is 0.7 μm, which lies within the measurement precision of the *XY* test bench.

4.4 Tilt performance

The tilt of the fiber relative to the reference, in this case the baseplate, can be measured directly at different positions in the workspace. The tilt of both axes and fiber relative to each other have to be estimated using a rigid body model of the positioner as mentioned in Section 4.2. In order to do so, each axis is moved individually to complete full circles at different positions of the other axis. Table 2 shows an example of results for one of the 10 prototypes. The fit of the model to measured points has an rms error of 0.016° which is just slightly larger than the precision of the tilt bench. This means that the rigid body model represents well the real positioner.

Table 2. Example of a tilt measurement.

Angles [deg]	Target	Measured	Difference
g–α (Orientation)	0	350.2	
g–α	0	0.033	0.033
α–β (Orientation)	180	203.2	23.2
α–β	0.11	0.046	0.064
β–f (Orientation)	180	167.7	12.3
β–f	0.24	0.208	0.032

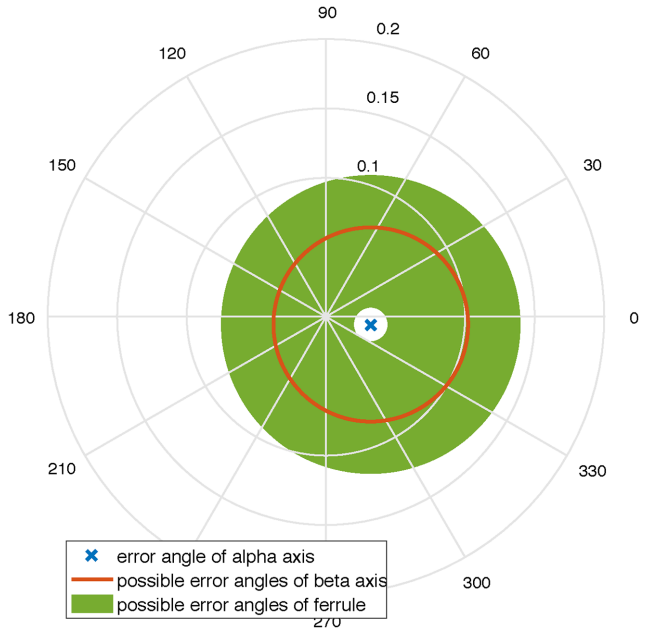

Figure 22. Example of tilt errors in all possible configurations.

Using the identified model of the positioner (including the relative tilts between the axes), it is possible to predict the total tilt error of the fiber in all possible configuration of the positioner. Fig. 22

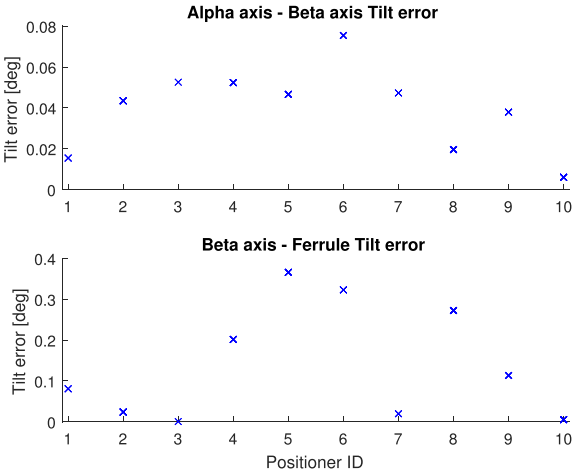

Figure 23. Tilt errors alpha–beta and beta–ferrule for the 10 prototypes.

shows all possible errors of the two axes and the ferrule for this positioner. The alpha axis has always the same tilt error as it doesn't move. The beta axis however is rotating around the alpha axis and its tilt error describes a circle around the tilt error of the alpha axis. The ferrule in turn rotates around the beta axis and its tilt error can be anywhere in the green surface. This example shows that the maximum tilt error is around 0.14°. This is the worst-case configuration of the positioner where all the tilt errors add up. In the best-case configuration, the three tilt errors cancel out and the tilt error of the fiber is 0°.

The alpha–beta and beta–ferrule tilt errors are shown for all 10 prototypes in Fig. 23. The ground–alpha tilt error is not reported because the fixation of the positioners on the test bench was not repeatable enough and therefore this measurement was not consistent. The average alpha–beta tilt error is 0.04° with a standard deviation of 0.02°. The average beta–ferrule tilt error is 0.14° with a standard deviation of 0.14°.

It has to be kept in mind that the tilt error requirement of 0.15° concerns the sum of these three errors. The alpha–beta tilt error of most positioners is of less than a third of the requirement. The beta–ferrule tilt error however lies over the overall tilt requirement for half of the positioners. This poor performance can be attributed to the ferrules themselves which show a misalignment of the fiber with respect to the outside diameter of up to several tenths of degrees. It is also possible that the two interfaces of the beta arm (to the beta axis shaft and ferrule) do not guarantee a good alignment in which case the interfaces have to be improved by making them longer or using a V-groove. It can be expected that the ground–alpha tilt error has a similar magnitude than the alpha–beta tilt error, because there is only one part involved (the base of the positioner) which has relatively large interface surfaces. The alignment of the alpha axis on one positioner was measured to be 0.03° using a coordinate-measuring machine during assembly.

These hypotheses have to be confirmed by additional tests using an improved interface on the test bench and measuring the tilt errors of the ferrules themselves.

4.5 FRD due to fiber stress

The throughput loss due to focal ratio degradation within the fiber is measured on one positioner. The throughput is compared between the fiber alone, the fiber in the positioner at minimal bending (beta arm folded in), and the fiber in the positioner at maximal bending (beta arm stretched out). The difference between the three cases is less than 1 per cent which is the accuracy of the measuring device. Further testing has to be done to confirm the requirement of 0.5 per cent.

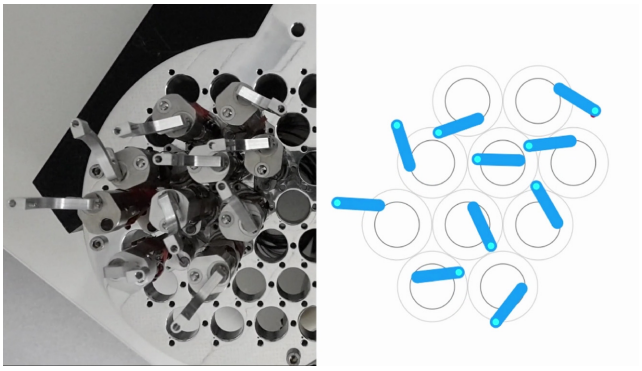

Figure 24. Snapshot of a collision avoidance test run. Right side: Simulation of trajectories at target positions. Left side: Execution of these trajectories with 10 prototypes. The full video can be seen at: https://youtu.be/Hc_Pr_hhaNA.

4.6 Collision avoidance

The collision avoidance algorithm has been validated on a sample of 10 positioners. The 10 prototypes are mounted on a test plate with 37 holes, arranged in a 25 mm pitched hexagonal pattern. The trajectories generated by the collision avoidance algorithm are sent to the positioners via the CAN bus described in Section 3.2.1. A broadcast CAN message then starts the movements on all positioners at the same time.

All the tested trajectories were successfully executed without collisions and the communication worked without problems. Fig. 24 shows the 10 prototypes at their assigned target locations.

4.7 Summary

Table 3 compares the obtained results with the requirements presented in Section 2. The mass of the positioner has been measured to be 164.5 g for the aluminium version including motors, electronics, and wiring. The operational temperature and humidity, max Z error and lifetime have not yet been tested.

5 CONCLUSION

The requirements for a fiber positioner system have been discussed and put in relation to the science objectives of the astrophysical survey. The design of a high density fiber positioning system for massive spectroscopic surveys has been presented. 10 positioner prototypes have been realized and tested on a custom-designed test bench. The tilt and positioning performances have been measured. It has been shown that the proposed design allows these positioners to accomplish their task for astrophysical surveys, in particular for the MOONS instrument on which its dimensions are based on. We highlight that our positioners are able to achieve the required precision without using an external metrology system and therefore the reconfiguration time is minimized. However, the operational temperature, and humidity, max Z error, lifetime, the ground–alpha and beta–ferrule tilt error still need further testing. Specially the assumptions about the beta–ferrule tilt error need to be verified.

Table 3. Fiber positioning requirements and achieved performance.

Need	Requirement	Value	Achieved performance
Pairwise observation	Focal plane coverage	Each position reachable by at least 2 positioners	Verified by design
Pairwise observation	Minimal fiber distance	4 mm	Verified by design
Telescope field of view and science goal	Pitch	25 mm	Verified by design
Target size	Size of the pupil	610 μm	Verified by design
Survey length	Lifetime	10^6 Movements/10 yr	
Science goal	Reconfiguration time	<30 s	25 s
Instrument efficiency	rms *XY* error	<20 μm	20 μm
Instrument efficiency	*Z* max defocus error	<50 μm	
Instrument efficiency	Max tilt error	±0.15°	cf. Section 4.4
Instrument efficiency	FRD due to fiber stress	<0.5% throughput loss	cf. Section 4.5
Instrument efficiency	Difference in focal ratio between fiber input and output	<1%	Verified by design
Environment temperature	Operational temperature	−10°C to +30°C	
Environment humidity	Operational humidity	5%–20%	
Low heat dissipation	Power while active	<2W	1.5 W
Low heat dissipation	Power while inactive	0 W	0 W
Earthquake resistance	Mass of the positioner	<200 g	164.5 g

Further work has also to be done to develop a consistent assembly process for mass production.

ACKNOWLEDGEMENTS

The authors would like to thank the Atelier de l'institut de génie mécanique (ATME) at EPFL for their support during the manufacturing phase of the prototypes, Hans Georg Limberger (EPFL) and Toralf Scharf (EPFL) for precious suggestions, Laleh Makarem, and Denis Gillet for the productive collaboration. The help of the UK Astronomy Technology Centre was much appreciated.

This research has been supported by the European Research Council advanced grant "Light on the dark" (LIDA) and the Swiss Commission of Technology and Innovation grant no. 17901.1 PFIW-IW between EPFL and Maxon Motor AG (Switzerland).

REFERENCES

Anderson L. et al., 2012, MNRAS, 427, 3435
Anderson L. et al., 2014, MNRAS, 441, 24
Cirasuolo M. et al., 2014, in Suzanne K. R., Ian S. M., Hideki T., eds, Proc. SPIE Conf. Ser., Vol. 9147, Ground-based and Airborne Instrumentation for Astronomy V. SPIE, Bellingham, p. 91470N
de Jong R. S. et al., 2014, in Suzanne K. R., Ian S. M., Hideki T., Proc. SPIE Conf. Ser., Vol. 9147, Ground-based and Airborne Instrumentation for Astronomy V. SPIE, Bellingham, p. 91470M
Delubac T. et al., 2015, A& A, 574, A59
Eisenstein D. J. et al., 2005, ApJ, 633, 560
Fahim N. et al., 2015, MNRAS, 450, 794
Fisher C., Braun D., Kaluzny J., Haran T., 2009, IEEE Aerospace Conference. IEEE, p. 1
Kimura M. et al., 2010, Publications of the Astronomical Society of Japan, Vol. 62. Oxford University Press, p. 1135
Makarem L., 2015, PhD thesis, EPFL, Lausanne
Makarem L. et al., 2014, in Gianluca C., Nicole M. R., eds, Proc. SPIE Conf. Ser., Vol. 9152, Software and Cyberinfrastructure for Astronomy III. SPIE, Bellingham, p. 91520Q
Makino H., Furuya N., 1980, in Proceedings of the First International Conference on Assembly Automation, p. 77
Ramsey L. W., 1988, ASP Conf. Ser., Fiber optics in astronomy, p. 26
Silber J. H. et al., 2012, in Ramón N., Colin R. C., Eric P., eds, Proc. SPIE Conf. Ser., Vol. 8450, Modern Technologies in Space- and Ground-based Telescopes and Instrumentation II. SPIE, Bellingham, p. 845038
Xing X., Zhai C., Du H., Li W., Hu H., Wang R., Shi D., 1998, in Larry M. Stepp, Proc. SPIE Conf. Ser., Vpl. 3352, Advanced Technology Optical/IR Telescopes VI. SPIE, Bellingham, p. 839

This paper has been typeset from a TEX/LATEX file prepared by the author.